American Mineralogist, Volume 78, pages 1246–1256, 1993

Early partial melting in pyroxenes

Nicole Doukhan, Jean-Claude Doukhan
Laboratoire de Structure et Propriétés de l'Etat Solide (URA CNRS 234), Université des Sciences et Technologies de Lille, 59655 Villeneuve d'Ascq-Cedex, France
Jannick Ingrin, Olivier Jaoul, Paul Raterron
Laboratoire de Géophysique et Géodynamique Interne (URA CNRS 1369), Université Paris-Sud, 91405 Orsay-Cedex, France

Abstract

Diopside annealed beyond critical conditions of temperature (T_c) and f_{O_2} exsolved tiny precipitates of a molten phase enriched in silica. T_c was markedly lower than the melting temperature T_M ($T_c \approx 1100$ °C, whereas $T_M \approx 1350$ °C for the composition studied). The size of the precipitates increased dramatically with temperature. The first detected nuclei had diameters of a few tens of nanometers and represented a volume proportion ≈0.01%. At 1250 °C, the mean precipitate size reached 300 nm, and the volume proportion was ≈0.2%. After a long annealing time at 1280 °C, the volume proportion was ≈5%, and the largest precipitates reached 1 μm. Furthermore, elongated melt veins extending over 50 μm also formed. The smaller precipitates were almost pure silica, then as they grew, their composition became progressively enriched in sodium, aluminum, calcium, and iron oxides. This early partial melting (EPM) phenomenon still occurred for annealings under confining pressure up to $P \approx 1.6$ GPa at $T \approx 1300$ °C. Similarly, EPM began at ≈1300 °C in experimentally annealed enstatite. Naturally annealed pyroxenes (clino- and ortho-) from xenoliths brought to the surface by volcanic explosions also exhibit similar precipitates enriched in silica.

Introduction

Fractional crystallization of magmas is relatively well understood, but that is not the case for the opposite phenomenon, i.e., the partial melting of a representative assemblage of mantle rocks. In particular, one does not know the relative influences of parameters like T, P, f_{O_2} or f_{H_2O}, and the mineralogical compositions of the rocks before and after partial melting. The mechanisms by which melt is extracted (percolation along grain boundaries, progressive ascent of this melt along crack networks, etc.) and their chemical evolution from the first appearance of melt to the beginning of the percolation process are also poorly documented by laboratory experiments. Until now, such experiments were more focused on researching equilibrium relationships between rocks and magmas than researching kinetic aspects. The very beginning of partial melting thus appears to be an especially important phenomenon to study experimentally.

Recent investigations of the properties of high-temperature creep of almost pure diopside single crystals (Raterron and Jaoul, 1991; Ingrin et al., 1991) have shown that the mineral begins to melt incongruently and to exsolve numerous tiny precipitates of a molten phase well below its liquidus temperature T_M (≈1350 °C, after the calibration proposed by Huebner and Turnock, 1980). In the above experiments, the initiation of melting was detected at a temperature as low as ≈1140 °C (at $f_{O_2} \approx 2 \times 10^{-17}$ MPa). The composition of the molten precipitates was enriched in silica. If the material is rapidly cooled to ambient temperature the precipitates become glass, but for slower cooling rates, the precipitates may either redissolve or evolve to a mixture of glass and crystallites of wollastonite $CaSiO_3$. Such tiny precipitates can be directly detected only by transmission electron microscopy (TEM), and that probably explains why they were not observed earlier. We called this phenomenon early partial melting (EPM). In the deformation experiments of Raterron and Jaoul (1991), EPM was indirectly detected through the interaction of the precipitates of melt with the mobile dislocations. When enough precipitates are nucleated they efficiently pin the mobile dislocations, thus hardening the material. Similarly, at least one of the boundaries between electrical conductivity regimes of diopside (Huebner and Voigt, 1988) can probably be ascribed to EPM.

Materials investigated

TEM investigations on the first stages of EPM were performed on three annealed pyroxenes: (1) a clinopyroxene with a composition close to pure diopside, on which numerous annealings were performed under controlled conditions (including P_{O_2}), with a view to inducing

0003–004X/93/1112–1246$02.00

EPM, (2) an orthopyroxene with a composition close to enstatite, on which a few annealings were performed, and (3) clino- and orthopyroxenes from a xenolith that was presumably annealed naturally in a magmatic chamber and that also has characteristic features of EPM. The first pyroxene is the same Russian gem-quality chromium diopside whose high-temperature creep behavior was studied by Raterron and Jaoul (1991) and in which Ingrin et al. (1991) discovered the glassy precipitates of EPM and their strong elastic interactions with the mobile dislocations. It was provided by Gebrüder Bank (Idar Oberstein, Germany). Its chemical composition, checked by electron microprobe, is $Na_{0.025}K_{0.001}Ca_{0.969}Mg_{0.970}Fe_{0.036}Mn_{0.001}Ni_{0.001}Cr_{0.013}Al_{0.007}Si_{1.985}O_{5.996}(OH)_{0.004}$. It is rather homogeneous and close to pure diopside (all the analyses presented below are normalized to six O atoms). The melting temperature (solidus) at atmospheric pressure for this composition is $T_M = 1350$ °C, after Huebner and Turnock (1980). H was detected through the infrared absorption of its associated OH groups, and its concentration was estimated from the area under the absorbance peaks by using the calibration of Wilkins and Sabine (1973). The infrared signature of these absorption peaks strongly suggests that H enters in specific sites of the lattice (Ingrin et al., 1989), and therefore it has to be taken into account in the chemical formula. It is indicated above under the rather arbitrary form of OH groups. It was shown, however, that most of this H disappears after annealing 70 h in Ar at ≈1100 °C (Ingrin et al., 1989). Like the previous ones, the crystals used in this study are slightly zoned. Specimens to be annealed were cut in the apparently defect-free zones. TEM observations performed in these good regions prior to the annealings revealed a low dislocation density ($<10^9/m^2$) and no other defects such as twins, inclusions, or precipitates.

The second pyroxene studied is a gem-quality orthopyroxene single crystal from Tanzania (provided by Becker, Idar Oberstein, Germany). The crystals are light brown, they appear free of any weathering, inclusions, or precipitates, and their mean composition is $Mg_{1.911}Fe_{0.067}Ca_{0.005}Mn_{0.006}Al_{0.017}Si_{1.992}O_{6.000}$. TEM investigations performed prior to the annealings revealed a low dislocation density ($<10^9/m^2$) and no other defects such as fractures, lamellae of weathered products or of clinoenstatite, as those often found in naturally deformed orthopyroxenes (Doukhan et al., 1986; Nazé et al., 1987).

The third type of pyroxene used to study EPM consists of clino- and orthopyroxenes from a pyroxenite xenolith brought to the surface by a volcanic eruption. The chemical composition varies slightly from grain to grain, but, as a general trend, the Fe content is appreciably larger than in the two previous pyroxene samples. The xenolith was collected in the old volcanic province of the French Massif Central. It most likely was annealed for a long time in a magmatic chamber at high temperature and low pressure (≈1250 °C and ≈500 MPa, see Berger and Vannier, 1984) before being carried toward the surface by magma ascent and quenched.

Experimental

The size, the spatial distribution, and the chemical composition of the precipitates and glass veins exsolved at high temperature in clino- and orthopyroxenes were investigated by analytical STEM (Philips CM 30 apparatus operating at 300 kV equipped with a Tracor X-ray energy-dispersive spectrometer attachment). Annealing experiments on diopside and enstatite single crystals were performed at various temperatures above 1100 °C and at partial pressures of O controlled to fix the Fe^{3+}/Fe^{2+} ratio at reasonable values (approximately within the olivine Fo_{95} stability field, see Nitsan, 1974). A number of samples were strained during annealing, especially the samples annealed at moderate temperature, because it appears that plastic deformation accelerates the nucleation of the precipitates and leads to a more homogeneous spatial distribution of the precipitates. This influence of plastic deformation on precipitation kinetics—especially on nucleation—might result from the presence of numerous dislocations acting as preferential nucleation sites.

Small blocks of diopside and enstatite 2 × 2 × 4 mm³, as well as thin sections (30 μm) polished on both faces, were prepared for annealing. As a general rule, the thin sections were annealed at the higher temperatures (>1250 °C), and the small blocks were annealed and underwent creep at the lower temperatures. Most of the annealings were performed in an apparatus for dead-load creep at 1 atm described in Raterron and Jaoul (1991) in which f_{O_2} is controlled by a continuous flow of a gaseous mixture of Ar, H_2O vapor, and H. This mixture buffers the partial pressure of O through the chemical equilibrium $H_2 + \frac{1}{2}O_2 \leftrightarrow H_2O$ with low partial pressures ($P_{H_2} \leq P_{H_2O} \leq 2.10^{-3}$ MPa). A few annealings were also performed in a piston-cylinder apparatus (Raterron, 1992) at a confining pressure up to 1.85 GPa. The corresponding samples were embedded in an Fe capsule to maintain a low f_{O_2} (close to the Fe + FeO buffer). The pressure medium was boron nitride, and the thermocouple regulating the temperature was located within ½ mm of the capsule. Temperature gradients were minimized, and T is known within ±5 °C. Samples were in most cases recovered intact, as transparent as before the experiment and unfractured. Sometimes they were slightly deformed, indicating that deviatoric stresses were superimposed on the confining pressure. Some cracks extending perpendicular to the loading piston axis were generated during unloading after thermal quench.

Precipitate size, density, and chemical composition

Diopside

Nucleation of EPM precipitates. In samples that were annealed and strained, EPM was detected by a decrease of the activation energy of the strain rate beyond critical conditions of temperature (T_c) and partial pressure of O ($P_{O_{2c}}$). This abrupt change in activation energy is assumed to result from the interaction between the mobile dislo-

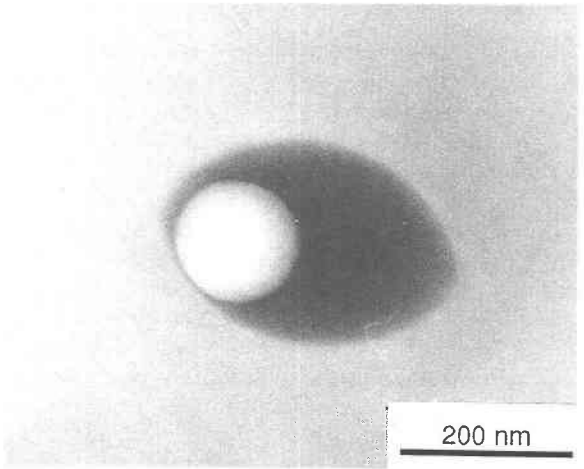

Fig. 1. Sample annealed and crept 500 h at 1104 °C with $P_{O_2} = 7 \times 10^{-18}$ MPa. Typical ellipsoidal precipitate with a spheric hole in its middle.

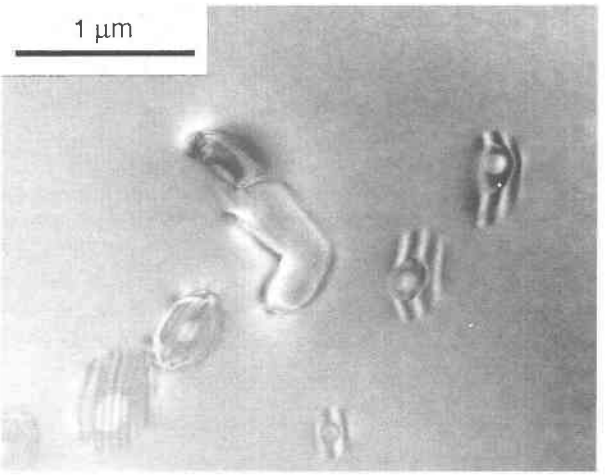

Fig. 2. Sample annealed 170 h at 1200 °C with $P_{O_2} = 1.4 \times 10^{-12}$ MPa. Tiny precipitates surrounded by an irregular fringe contrast pattern, which may be due to local chemical changes in the matrix.

cations and the precipitates. The creep experiments of Raterron and Jaoul (1991) yielded the following critical values: $T_c = 1140$ °C and $P_{O_{2c}} = 2 \times 10^{-17}$ MPa. The very beginning of EPM may start, however, at slightly lower values, but with a size and a density of precipitates too small to interact markedly with dislocations. We have thus also investigated by TEM samples that underwent creep at T and P_{O_2} conditions slightly lower than the above critical values. The first evidence of EPM was detected in a sample that exhibited a normal creep behavior (no change in the creep activation energy). We detected by TEM small, faint, contrast features with a highly heterogeneous density. Large areas are free of defects, whereas in other samples the density reaches $\approx 10^{16}/m^3$. As almost all these contrast features are very small (≤ 100 nm in bright field), it was not possible to elucidate unambiguously the origin of the contrasts observed, except for the biggest ones, which reach ≈ 300 nm (Fig. 1). These are ellipsoidal precipitates of an amorphous phase (no extra spots in the diffraction patterns). They are detected easily only in bright field, where they appear darker than the surrounding matrix, whatever the diffracting conditions. This is the contrast expected for an amorphous precipitate that diffuses the incident beam regardless of its orientation (this diffused energy is subtracted from the transmitted beam, and, as a result, the amorphous region appears darker than the crystalline matrix). We systematically observed a perfectly spherical hole in the middle of these precipitates with a volume estimated to be one-seventh of the total volume. No stress field was detected around these precipitates, whatever their size. As the sample was cooled relatively slowly, it is reasonable to assume that, if a stress field occurred around the precipitates, it relaxed during cooling. It is not easy to perform quantitative X-ray microanalyses on such small precipitates because they are almost always embedded in the diopside matrix. We thus performed microanalyses on "sandwiches" contained one amorphous precipitate embedded in the diopside matrix. Such analyses, which integrate a large proportion of diopside matrix together with the small precipitate, indicate a slight but unambiguous enrichment in silica. The tiny precipitates must thus be markedly enriched in SiO_2. The situation as observed by TEM is essentially similar for samples annealed and undergoing creep at conditions just above the critical conditions T_c and $P_{O_{2c}}$ indicated above, except that the precipitates become pervasive, more numerous and larger, and they interact with dislocations. Microanalyses performed on sandwiched precipitates still indicate an enrichment in SiO_2.

Evolution with increasing temperature. Annealing plus creep at higher temperatures (≈ 160 h at 1200 °C and $f_{O_2} = 1.4 \times 10^{-12}$ MPa) induced a larger and more homogeneous density of precipitates, with a mean size ≈ 250 nm and a density $\approx 3 \times 10^{17}/m^3$. Their volume fraction reached $\approx 0.2\%$. Most of them were surrounded by dislocation loops, which enclosed a faint fringe pattern contrast. Even when the precipitates are not surrounded by dislocation loops one can observe, with diffraction conditions with low indices, a weak fringe pattern surrounding the precipitates (Fig. 2). We believe that this contrast results from chemical changes in the immediate vicinity of the precipitates or in the areas limited by the dislocation loops. We also believe that these loops are nucleated in response to the elastic stresses around the precipitates (such stresses are caused by differences in specific volumes between the precipitated amorphous phase and the crystalline diopside matrix). This situation is somewhat similar to the one observed in wet quartz and wet berlinite ($AlPO_4$), in which tiny bubbles of H_2O precipitate during annealing at moderate confining pressure. As soon as the H_2O bubbles were large enough (≈ 20 nm), they nucleated a sessile dislocation loop, which relaxed the inner

bubble pressure (Boulogne et al., 1988; Cordier and Doukhan, 1989). By selecting the larger precipitates located in the thinner region of the specimen (close to the edge of the thin foil), we were able to analyze the amorphous phase in the precipitates. When we compared them with the original diopside matrix, we found an appreciable enrichment in Si and in Na, Al, and Fe on the one hand and an almost complete depletion in Mg on the other hand. The concentration of Ca decreased but did not vanish. The composition of these precipitates no longer corresponded to a clinopyroxene formula. For example, we found the following composition for a large precipitate: $Mg_{0.095}Fe_{0.142}Ca_{0.532}Al_{0.095}Na_{0.152}Si_{2.506}O_{6.000}$.

Comparison between a sample having undergone creep and annealed and one just annealed (both 10 h at T = 1250 °C, $f_{O_2} = 5.2 \times 10^{-16}$ MPa) shows that plastic deformation still plays a relevant role on the homogeneity of the spatial distribution of precipitates at this temperature. In the sample just annealed, the density of amorphous precipitates is not homogeneous. By contrast, in the sample crept and annealed, the size and the density of precipitates were more homogeneous (density $\approx 7 \times 10^{17}/m^3$ representing a mean volume fraction ≈0.2%).

In the sample annealed for 80 h at T = 1300 °C and $f_{O_2} = 2 \times 10^{-10}$ MPa, the precipitates exhibited a homogeneous density ($\approx 4 \times 10^{17}/m^3$) and size (≈400 nm) that represent a volume fraction ≈1%. In selecting the bigger precipitates located in the thinner regions of the specimen, we could characterize the concentration profiles for the major elements in the surrounding matrix by performing a series of X-ray microanalyses along a line cutting the precipitate (Fig. 3). We clearly detected a marked enrichment in silica in the amorphous phase. Furthermore, the surrounding crystalline matrix appeared much more sensitive to electron-beam irradiation than standard diopside. This effect was detected at distances up to 2–5 μm from the precipitates. In these regions, the compositions provided by the X-ray microanalyses evolve with increasing electronic density on the analyzed area. The divalent cations Mg and Ca migrated from the area under the beam. The corresponding concentration profiles have thus to be considered with extreme care. These experiments thus reveal that the diopside material around the precipitates could have a slightly different composition or at least a different cationic site occupation, allowing high cationic mobility although its crystallographic structure (i.e., its diffraction patterns) looks unaffected. Diffraction contrast experiments do not reveal any change either, except the weak fringe contrast mentioned above. The observed higher mobility of the divalent cations, which diffuse under the electron beam, suggests that the material or at least its cationic sublattice might be partially disorganized and more sensitive to irradiation damage than typical diopside.

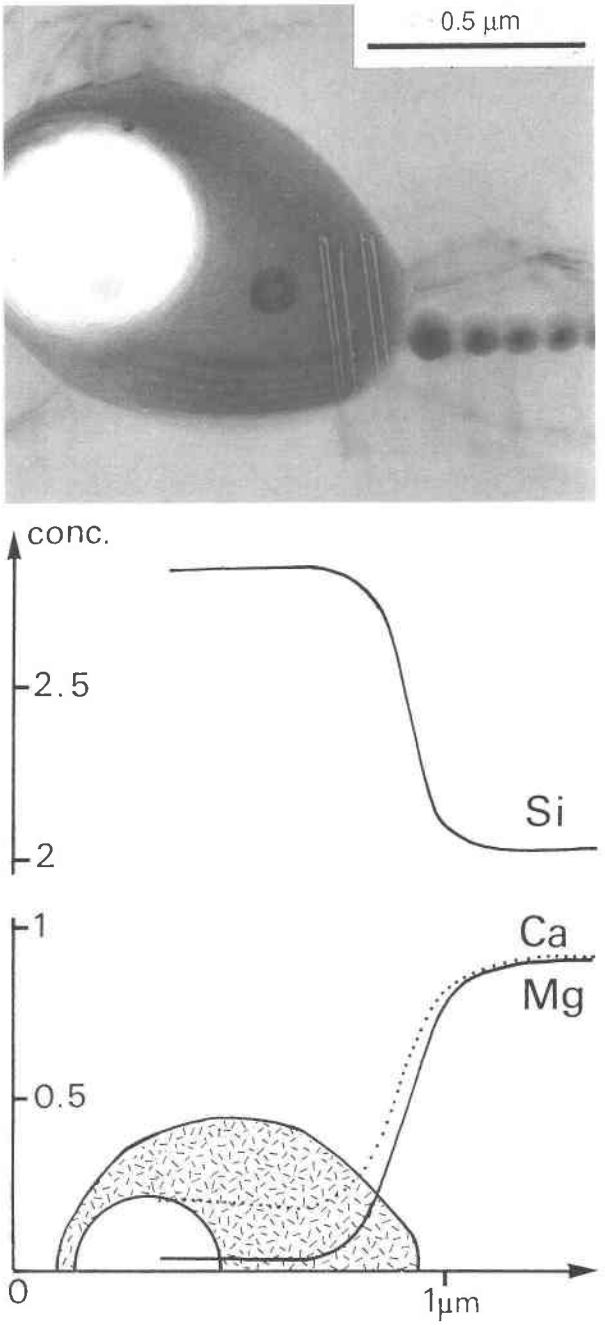

Fig. 3. Annealing at 1300 °C. Tentative determination of the concentration profile in the vicinity of a large precipitate. The dark contamination spots indicate the positions of the analyses (atomic concentrations for six O atoms).

Evolution with increasing annealing time at given temperature. The above experiments show that the evolution of EPM with increasing temperature affects the size (and consequently the volume fraction) rather than the density of precipitates. The volume fraction of the amorphous phase increases, at given temperature, with the duration of annealing, and one can expect that it should reach a limit corresponding to its thermodynamic equilibrium. We tested this possibility by performing longer annealings. By heating a sample at 1200 °C and $f_{O_2} = 10^{-14}$ MPa for 150 h, we found a volume fraction of precipitates as

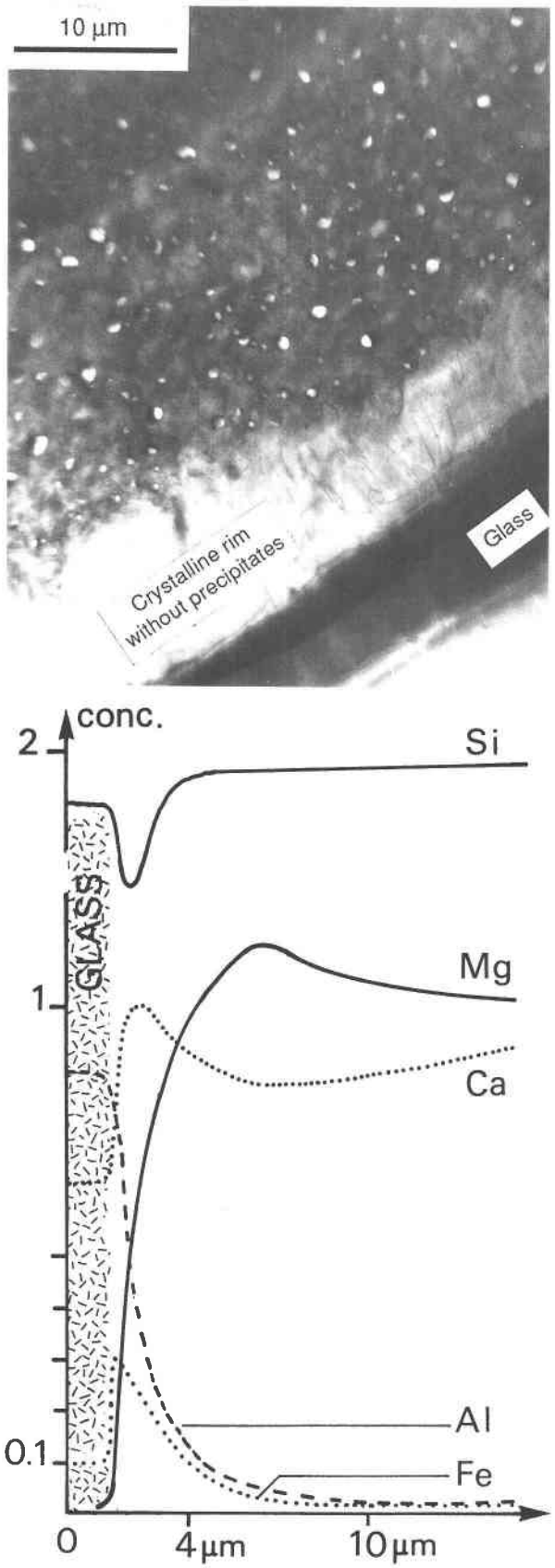

large as ≈3% (to be compared with the corresponding value of 0.2% for 60 h at the same temperature and $f_{O_2} = 1.4 \times 10^{-12}$ MPa). Along the same lines, annealing plus creep during ≈300 h at 1260 °C and $f_{O_2} = 5 \times 10^{-12}$ MPa leads to a volume fraction of amorphous material of ≈5%, to be compared with 0.2% for only 10 h at $f_{O_2} = 5 \times 10^{-15}$ MPa (but this latter comparison raises the problem of the possible influence of f_{O_2}, which was lower in the short duration experiment). Furthermore, with increased annealing time two new types of precipitates are seen:

1. In addition to the usual spheroidal amorphous precipitates we find a few very elongated veins of amorphous material. They extend over at least 50 μm, with a width on the order of a few micrometers (Fig. 4). Because of their large volume, these veins could represent the major part of the volume of the amorphous phase precipitated. The diffraction patterns performed on the crystalline rims are identical to those of the bulk diopside structure and indicate identical orientation, but the rims are completely depleted of spheroidal precipitates. These are detected again a few micrometers farther away with a large and homogeneous density and a mean size ≈1 μm. The spatial configuration of the veins is more favorable than the configuration of the small precipitates for recording concentration profiles because the enhanced sensitivity to electron beam damage can be bypassed. One can reasonably assume that the concentration profiles only depend on the distance perpendicular to the vein rim (i.e., there should be a translation symmetry along the vein direction). Analyses can thus be performed on elongated areas parallel to the rim with the STEM mode. This technique appreciably reduces the electron beam density, and consequently the possible irradiation-induced change of the chemical composition during the analyzing process. Several concentration profiles have been recorded in various places along the veins. They all are very similar. They must be representative of the element distribution perpendicular to the rim. A typical profile is shown in Figure 4. It shows that the amorphous material in the vein is highly enriched in Al and almost completely depleted in Mg (composition $Mg_{0.018}Fe_{0.102}Ca_{0.608}Na_{0.187}K_{0.048}Al_{0.868}Si_{1.925}O_{6.000}$). The crystalline rims of the vein are still clinopyroxene, as demonstrated by their diffraction patterns, but they are pathologic from a chemical point of view. The chemical composition in the rim varies appreciably with the distance to the vein. In its immediate vicinity, the major element composition can be written using the usual rules of pyroxene crystal chemistry for the 1:1 partition of the Al cations between the octahedral and the tetrahedral sites, $Mg_{0.43}Fe_{0.26}Ca_{0.95}Al_{0.29}[Al_{0.29}Si_{1.74}]O_6$ (Cameron and Papike, 1980).

←

Fig. 4. Sample annealed and crept 300 h at 1260 °C. Amorphous vein bounded by rims of crystalline material without glassy precipitates. The concentration profiles are indicated for the major elements (atomic concentrations for six O atoms).

2. The second type of precipitate presents the same usual spheroidal shape and has a similar size (≈1 μm), but these precipitates are partially filled with crystalline material, as shown by diffraction patterns. Some remnant glassy material, however, still occurs in the precipitate cavities. In selecting precipitates in thin regions, close to the edge of the sample, we could determine their composition. It is close to $CaSiO_3$, with some impurities, which might stem from contamination by the neighboring matrix. For instance, the crystallite shown in Figure 5 yields the composition $Mg_{0.10}Fe_{0.03}Ca_{1.89}Si_{1.98}O_{6.00}$. Detailed analysis of the diffraction patterns of the crystallites is consistent with triclinic wollastonite (lattice parameters a = 0.794, b = 0.732, c = 0.707 nm, α = 90.03, β = 95.37, and γ = 103.43°, after Buerger, 1956). Many such wollastonite crystallites are detected in precipitate pockets, and they all have the same crystalline orientation. As wollastonite is known to crystallize rapidly, this observation strongly suggests that these wollastonite crystallites grew from the melt in epitaxial relation with the matrix, during the slow cooling stage. Such an assumption is supported by the fact that the faces of the crystallites are low index planes [(001), (010), (101), (10$\bar{1}$), see Fig. 5]. No epitaxial relationship was found between those wollastonite crystals and the host diopside, except that $[110]_{diop}$ is approximately perpendicular to $(100)_{wol}$. It is well known, however, that several wollastonite polymorphs and epitaxial relations might have occurred at the crystallization temperature, between the matrix and the $CaSiO_3$ polymorph that epitaxed at high temperature and then reverted to the triclinic form observed here during subsequent cooling. We could not determine precisely the composition of the remaining glass because it is more rapidly ion thinned than the other materials (glass in the previous precipitates, wollastonite, or diopside), and, as a consequence, only very small amounts of it remain in the cavity and are almost systematically embedded in the matrix.

Influence of the confining pressure. We also performed a few annealing experiments under confining pressure to determine if the precipitation of an amorphous phase still occurs at similar temperatures. The piston-cylinder equipment used (Raterron, 1992) allows the specimens to be quenched very rapidly. Samples in pure Fe capsules are cooled to room temperature in approximately 1 min. Thus the precipitate microstructures must be representative of high temperature, except that the molten precipitates are quenched to glass. Annealings of 2½ h at 1300 °C were performed at P = 0.5, 1.5, and 1.85 GPa, respectively, under f_{O_2} conditions thought to be that of the Fe + FeO buffer. In the sample annealed at 0.5 GPa, one still detected precipitates with a rather heterogeneous density of $(5 \times 10^{16}$–$10^{17})/m^3$. Their size is quite small (≈100 nm, see Fig. 6a) and their volume proportion is <0.1%. In contrast with samples annealed at ambient pressure followed by a slow cooling, the precipitates are now systematically surrounded by a strong elastic strain field, which is often partially relaxed by dislocation loops.

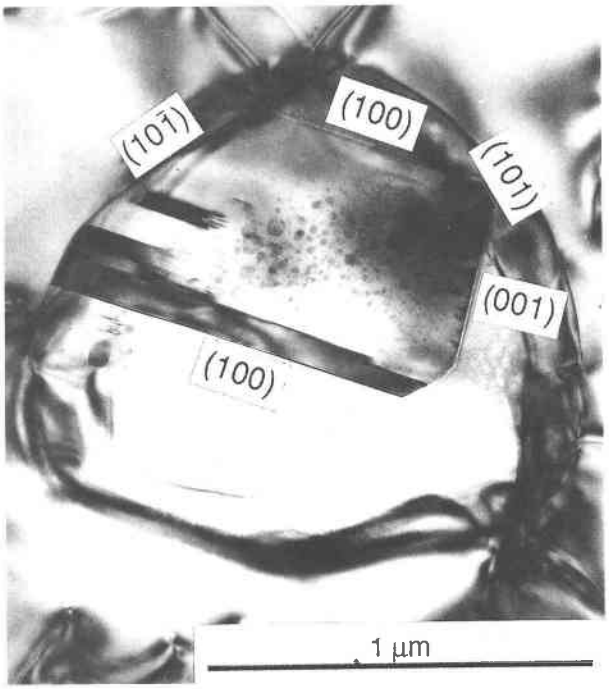

Fig. 5. Same sample as in Fig. 4. Large spheroidal precipitate with a twinned crystallite of wollastonite [twin boundaries parallel to $(100)_{wol}$] grown in it. The low index faces of the crystallite strongly suggest crystallization from the melt.

In the sample annealed at P = 1.5 GPa, the density of precipitates became very low and extremely heterogeneous, with large areas free of precipitates. The regions in which precipitates are detected systematically exhibit a large density of dislocations and mechanical twins, which clearly indicate that some plastic deformation occurred (Fig. 6b). This plastic deformation most probably stems from the nonhydrostaticity of the high confining pressure, and it most certainly had a catalytic effect on the nucleation of the precipitates. These precipitates are extremely small, but it is impossible to precisely determine their size because of their large surrounding stress field. These must represent a very low volumic fraction (<0.01%?). The third specimen, annealed at 1.85 GPa, exhibited no EPM feature. Hence the limit for EPM at 1300 °C is constrained between 1.5 and 1.85 GPa in the Fe + FeO buffering conditions, at least for the crystal studied with an Fe concentration Fe/(Mg + Ca + Fe) ≈ 0.02. At ambient pressure, this limit, determined by the abrupt change of the activation energy, is T = 1140 °C, with $f_{O_2} = 2 \times 10^{-17}$ MPa, but, as shown by our TEM investigations, the very beginning of EPM starts at slightly lower values ($T \geq 1104$ °C, $f_{O_2} \geq 7 \times 10^{-18}$ MPa).

Enstatite

We performed annealing experiments at ambient pressure on orthopyroxene with a low Fe content. The same procedure was used to control f_{O_2}. No precipitation was detected for annealing at $T < 1300$ °C, $f_{O_2} \approx 10^{-16}$ MPa.

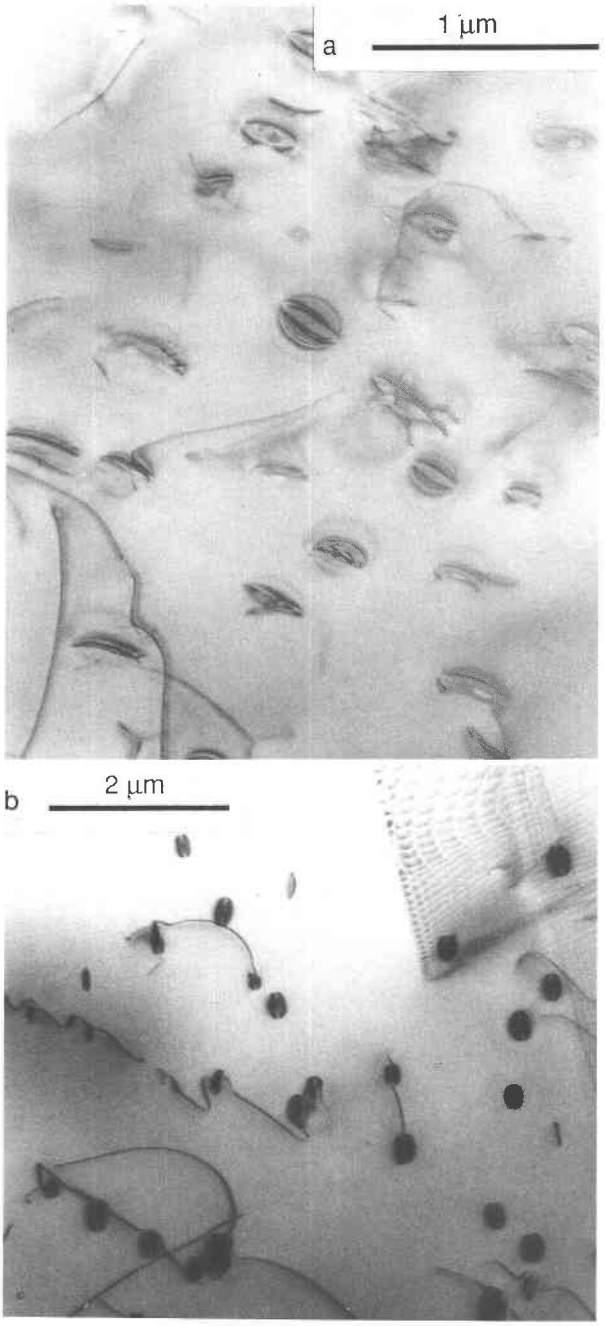

Fig. 6. Annealing at 1300 °C under solid confining pressure. (**a**) P = 0.5 GPa. The small amorphous precipitates are surrounded by an elastic strain field (ellipsoidal contrast) and dislocation loops. (**b**) P = 1.5 GPa. Area plastically deformed with dislocations and thin mechanical twin lamellae (upper left, visible by the twin dislocations in the boundaries). The tiny precipitates preferentially nucleated on the dislocations. They are smaller than at 0.5 GPa and also surrounded by a strain field.

After annealing 24 h at T = 1300 °C, $f_{O_2} \approx 10^{-15}$ MPa, the most prominent defect microstructure consists of a huge density of very thin lamellae of clinoenstatite (CEn, space group $P2_1/c$). These thin lamellae were presumably

Fig. 7. Orthoenstatite annealed 24 h at 1300 °C, $f_{O_2} = 10^{-15}$ MPa. The precipitates have the same ellipsoidal shape with a small spheric hole in their middle as those found in diopside but they are smaller for comparable annealing conditions.

induced by the large stresses generated by the transformation of orthoenstatite (OEn) into protoenstatite (PEn) during heating, or during the reversion of PEn → OEn during cooling (Kirby, 1976; Doukhan et al., 1986). We tentatively used diffraction conditions, putting the CEn lamellae out of contrast for the observation of the tiny precipitates. We also observed the few regions between fractures that are free of CEn lamellae (the stresses generated during PEn reversion are relaxed in some areas by fracturing). In both cases we detected tiny precipitates very similar to the ones found in annealed diopside. They are ellipsoidal, with a small, perfectly spheric hole in their middle (Fig. 7). They must also be amorphous because no extra spots were found in the corresponding diffraction patterns. They are heterogeneously distributed, and some regions seem defect free. After annealing for 24 h at T = 1400 °C, $f_{O_2} \approx 10^{-15}$ MPa, the situation is essentially similar, except that the precipitates are larger. We were not able to determine correctly the chemical composition of the amorphous phase in the precipitates because they are embedded in the matrix. Semiquantitative microanalyses (performed with the sandwich technique described above) indicated however that, as for diopside, this amorphous phase is enriched in silica. The volume proportion of the amorphous phase is appreciably lower in annealed enstatite than in annealed diopside for comparable temperatures.

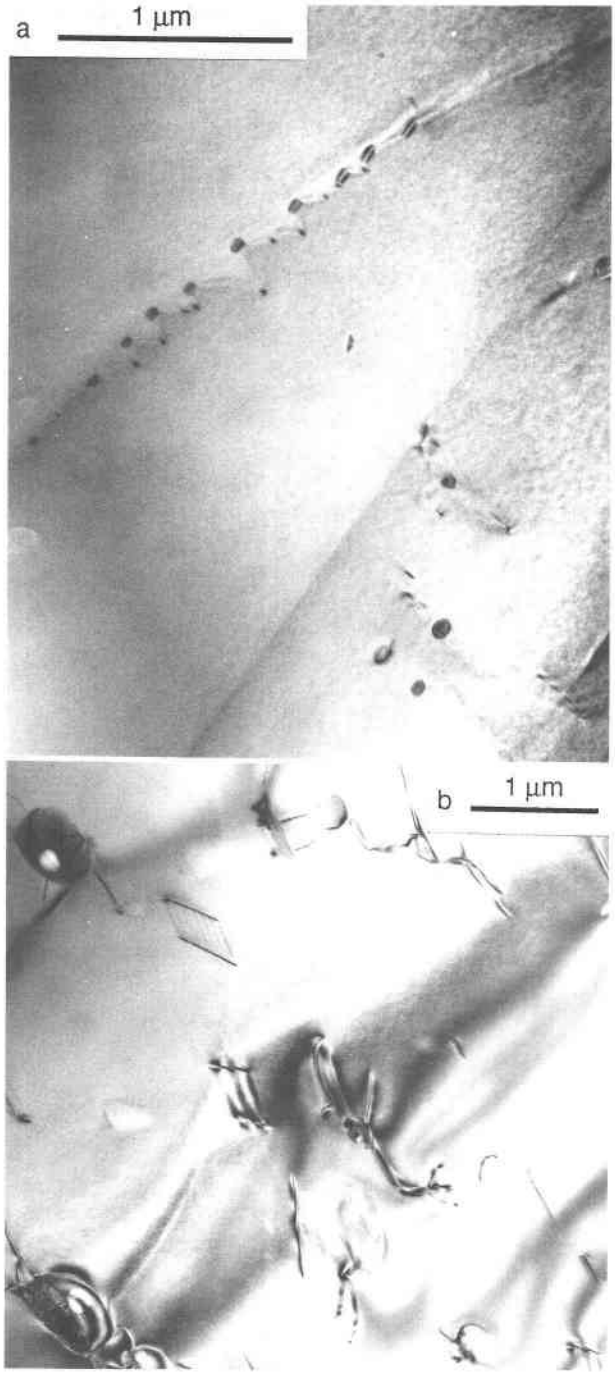

Fig. 8. Orthopyroxene from a xenolith from the French Massif Central. (**a**) Dislocations pinned by tiny amorphous precipitates (the dislocation is out of contrast, but still visible owing to its weak residual contrast). (**b**) Larger precipitates with small spheric holes in their middle.

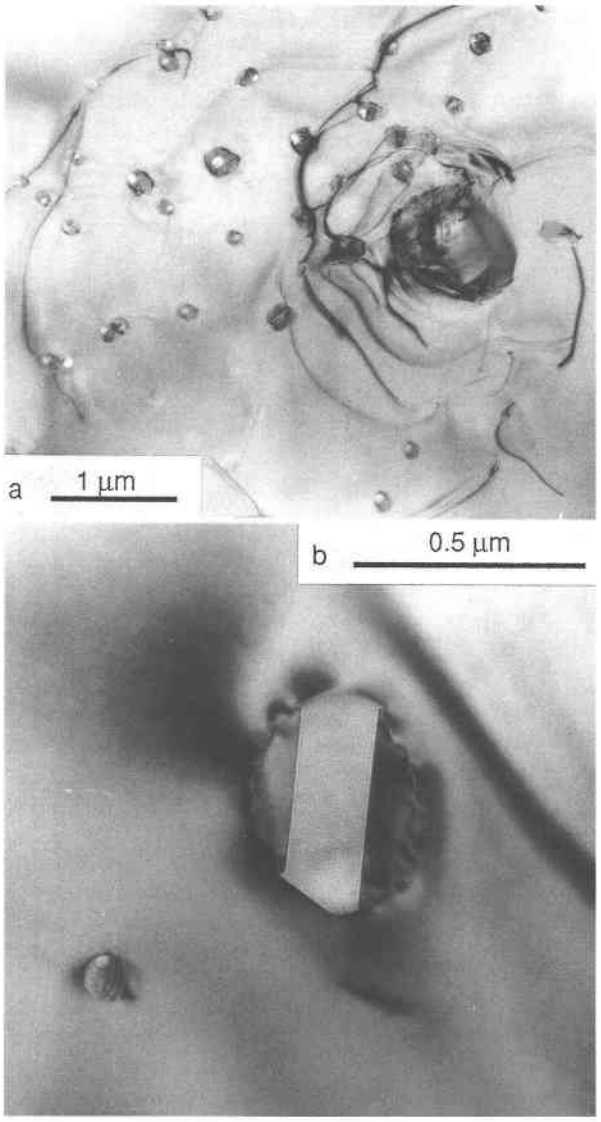

Fig. 9. Clinopyroxene from the same xenolith as in Fig. 8. (**a**) Tiny amorphous precipitates. (**b**) Crystallite grown from the melt in the precipitate cavity during cooling.

Naturally annealed pyroxenes

This xenolith material was collected in the volcanic province of the French Massif Central. No exsolution of clinopyroxene in the orthopyroxene crystals or orthopyroxene in the clinopyroxene crystals is found, in agreement with the general model of the rapid ascent of xenoliths during a volcanic explosion, followed by a rapid quenching at the Earth's surface. The tiny amorphous precipitates observed in both clino- and orthopyroxenes should have precipitated during the long residence of the rock at high temperature, in the magmatic chamber or in its immediate vicinity. The shapes, sizes, and spatial distributions of the EPM precipitates are very similar to those observed in experimentally annealed diopside and enstatite. Depending upon the grain studied, the sizes of the amorphous precipitates vary appreciably. It is reasonable to assume that such differences stem from slight differences in chemical compositions of the pyroxene matrix, but the small number of grains studied so far does not allow quantitative relationships to be inferred.

In an orthopyroxene grain with the composition

$Mg_{1.44}Fe_{0.38}Ca_{0.07}Mn_{0.01}Cr_{0.01}Ti_{0.01}Al_{0.07}Si_{1.91}O_{6.00}$, the tiny amorphous precipitates seem to have preferentially nucleated on dislocations, which in turn became pinned on the precipitates (Fig. 8a). In another orthopyroxene grain the amorphous precipitates are more homogeneously distributed, and they have the usual ellipsoidal shape, with a spheric hole in their middle (Fig. 8b). Qualitative microanalyses showed once again a marked enrichment in silica.

Similarly, Figure 9a is representative of the size and spatial distribution of the amorphous precipitates (connected to dislocations) in a clinopyroxene grain with composition $Mg_{0.778}Fe_{0.272}Ca_{0.691}Na_{0.042}Al_{0.373}Si_{1.834}O_{6.000}$. One still observes within most of them the typical spheric hole. As in the case of experimentally annealed diopside, one observes tiny crystallites (Fig. 9b) inside some of the larger precipitates. Unfortunately, because of their small size and their almost always being embedded in the surrounding matrix, it was not possible to determine the respective compositions of the crystallites and the remaining glass in these precipitates.

Discussion

The observations reported here clearly show that small amounts (volume proportion $\approx 0.01-\approx 5\%$) of a melt are produced in both clino- and orthopyroxenes heated at temperatures markedly below their widely accepted melting (solidus) temperature. The compositions of the molten phases differ from those of the original and the residual solids, i.e., pyroxenes melt incongruently. EPM occurs beyond a critical set of temperature and f_{O_2}. The data reported here show that the nuclei have a highly silicic composition, then they evolve toward a modal proportion and composition that depend on temperature and f_{O_2} (and confining pressure?). All the pyroxenes investigated here bear some Fe in the octahedral sites, and the f_{O_2} must control the Fe^{2+}/Fe^{3+} state. A point defect model recently developed by Jaoul and Raterron (1993) predicts that the higher the f_{O_2}, the more cationic vacancies should form (in both octahedral and tetrahedral sites). The resulting negative charges are electrically compensated by an increase in the concentration of Fe^{3+} at the expense of the Fe^{2+} in octahedral sites. There is, however, a limit to this process, and above a critical f_{O_2} (at given T and P) the pyroxene lattice can no longer accommodate this increase. Therefore SiO_2 begins to precipitate. This model allows the prediction of the thermodynamic conditions (essentially T and f_{O_2}) at which an almost pure silica phase should begin to precipitate. The amount of precipitate depends on the initial amount of Fe^{2+} cations in octahedral sites and on the initial concentration of vacancies. Such a model probably renders an accurate account of the nucleation stage. For long annealings, however, the precipitates grow, and their composition appreciably evolves. Another model should thus be developed for describing the evolution of the liquid phase. The preliminary data reported here only deal with a general evolutionary trend of the morphology and the chemical composition of the exsolved molten phase, but the final amount and equilibrium composition of this exsolved phase is not known. Therefore no refined model can be developed at the moment. Longer annealing experiments will be necessary to determine equilibrium chemical compositions of the precipitates in both clino- and orthopyroxenes, as a function of the initial compositions and of the thermodynamic conditions of annealing. Annealing under controlled activities of other components of the system (especially silica?) could also be useful.

EPM is not restricted to pyroxenes. Indeed an analogous point defect model has been proposed by Nakamura and Schmalzried (1983) for interpreting the early precipitation of SiO_2 in annealed fayalite, the Fe_2SiO_4 olivine. The same kind of analysis was also used by Jaoul et al. (1987) to interpret their observations of the exsolved silica-rich phases in olivine $Mg_{1.8}Fe_{0.2}SiO_4$. Furthermore, EPM that is believed to be controlled by the presence of Fe should be distinguished from two other phenomena: (1) the conventional incongruent melting (CIM) of end-member pyroxenes, and (Fe free) enstatite and diopside, and (2) the phenomenon called premelting, also detected in several pure end-member silicates.

CIM (of pure end-members free of oxidizable elements like Fe) arises at temperatures markedly higher, by at least 100 °C, than the ones reported for the onset of EPM. In pure enstatite, $Mg_2Si_2O_6$ CIM is known for many years to occur at ambient pressure at $T = 1557$ °C, leading to a SiO_2 liquid in equilibrium with forsterite (see, for instance, Huebner and Turnock, 1980). CIM was first detected in pure diopside by Biggar and O'Hara (1969) and then confirmed by Kushiro (1973), who found a temperature range of incongruent melting extending over 42 °C below the nominal melting temperature (1393 °C, after Kushiro, 1972). The microprobe analyses performed by Kushiro (1973) indicated a liquid composition enriched in $CaSiO_3$ and SiO_2, whereas the remaining solid was correspondingly enriched in Mg_2SiO_4 or $MgSiO_3$ (see also Morse, 1980). The common features between CIM and EPM are the formation of a SiO_2-rich phase (at least at the onset of EPM). The nucleation temperatures, however, differ, and that is not surprising if one remembers that EPM occurs in minerals containing substitutional Fe and other elements such as Al and Na, which are known to deeply depress the solidus curves (Huebner and Turnock, 1980). We tentatively suggest that CIM and EPM would have a common origin: in both cases the nonstoichiometry of pyroxenes would be accommodated by cation vacancies (octahedral and tetrahedral) with f_{O_2}-dependent concentrations, but these concentrations could become appreciably larger in Fe-bearing pyroxenes if enough Fe^{2+} were able to transform into Fe^{3+}, thereby compensating for the negative charges introduced by the cationic vacancies. In the absence of Fe (pure end-members) the extra negative charges related to the cation vacancies could only be compensated by electronic holes in the valence band; hence the possibility of charge balancing would become restricted to narrower temperature or f_{O_2} ranges. CIM as well as EPM can markedly affect a

number of macroscopic properties. This is the case with the creep experiments performed on diopside by Raterron and Jaoul (1991), in which the occurrence of EPM resulted in a relative hardening of the mineral due to the pinning of the mobile dislocations by the droplets of melt. As recently suggested by Jaoul and Raterron (1993) the high-temperature electrical conductivity of diopside (Huebner and Voigt, 1988) is another macroscopic property sensitive to the point defect population and consequently to EPM, which is believed to provoke a change in the conductivity behavior at low P_{O_2}.

Ziegler and Navrotsky (1986) and Lange et al. (1991) detected anomalous behavior of the heat capacity of pure diopside below its previously reported solidus temperature. They attributed this phenomenon to partial melting and extended the temperature range of incongruent melting of pure diopside to 59 °C below its nominal liquidus. Richet and Fiquet (1991) also detected an anomalous behavior of the specific heat of pure diopside from temperatures 100 °C below its nominal liquidus. This anomaly cannot be attributed to CIM or EPM, as demonstrated by the TEM investigations of Richet et al. (1992), who find no droplets of melt in their samples. These authors suggested, instead, that this behavior stems from structural modifications, which would more specifically affect the cationic sublattice. This anomalous phenomenon, called premelting, was recently detected in a large class of silicate minerals at high temperature (see for instance Richet and Bottinga, 1984; Richet and Fiquet, 1991). Richet and Fiquet (1991) suggested that the cationic sublattice would become molten or disordered. For instance, normal pyroxenes are characterized by a 100% occupation of the so-called M1 and M2 octahedral sites of the structure by the divalent cations while the remaining M3 sites are empty; in contrast, in the disordered structure these M3 sites would become available to the divalent cations, thus considerably enhancing their mobility. Our observation of an anomalously large sensitivity to irradiation damage (i.e., enhanced mobility of the cations) in the immediate vicinity of melt droplets could be interpreted by a similar disordered cationic sublattice. This cationic disorder would, however, be restricted to these disturbed zones.

The large glassy veins, like the one shown in Figure 4, might have a chemical composition close to equilibrium because they formed during the longest annealing experiment at high temperature. It is thus interesting to note that the Al concentration in the rims increases markedly from $\approx$0.01 in the bulk diopside, far from the vein, to values close to 0.6 in the immediate vicinity of the glass vein. As the vein is appreciably enriched in Al, one would have rather expected a marked Al depletion in the rims, which is not observed. These concentration profiles thus suggest that the growth mechanism of the glass veins is controlled by the mobility of its boundaries in a medium that should first become enriched in Al, Na, and Fe and impoverished in other elements, like Mg, rather than by the diffusion of the Al cations in the crystalline matrix toward the vein. There is however another possible interpretation, which cannot be discarded. Indeed, the concentration profiles may look inverted just because they would correspond to a state where the vein had already started to redissolve into the crystalline matrix, a process that would occur during the cooling stage that followed the end of the annealing experiment (to avoid thermal fracturing the sample is cooled from 1260 to 700 °C in $\approx$1 h). With great care one could thus interpret the recorded concentration profiles as evidence of the reversibility of the EPM phenomenon. The reverse process, affecting the concentration profiles over distances of a few micrometers, could be a relatively fast diffusion process, for it occurs within a highly chemically disturbed zone.

Conclusions

EPM appears to be a common feature in a variety of pyroxenes and may exist over a wide range of temperature, up to 200 °C below the nominal melting temperature, at least in Fe-bearing pyroxenes. The initial composition of the molten phase is very rich in silica, but it clearly evolves as EPM proceeds toward an enrichment in Al, Fe, and alkaline (Na and K), while the droplets become depleted in Mg. The influence of thermodynamic parameters like T and f_{O_2} on the composition of the first droplets seems to be at least qualitatively understood. Further growth of the precipitates and their chemical evolution toward equilibrium remain to be studied further before a model can be proposed.

Acknowledgments

We acknowledge E. Berger (Laboratoire de l'Ecole des Mines, Orléans) for kindly providing the xenolith material from the French Massif Central. We are pleased to thank F. Elie (Université Paris-Sud, Orsay), who performed the annealings under pressure. We also thank S. Huebner for a number of useful suggestions during the reviewing process of this manuscript. This work was financially supported by a contract from the DBT committee no. 4 (Fluides, Minéraux et Cinétique). This is an INSU-DBT contribution no. 633.

References cited

Berger, E.T., and Vannier, M. (1984) Petrology of megacrysts, mafic and ultramafic xenoliths from the pipe of eglazines, Causses, France. In J. Kornprobst, Ed., Kimberlites. I. Kimberlites and related rocks, p. 155–168. Elsevier, Amsterdam.

Biggar, G.M., and O'Hara, M.J. (1969) Solid solutions at atmospheric pressure in the system CaO-MgO-SiO_2 with special reference to the instabilities of diopside, akermanite and monticellite. Progress in Experimental Petrology, First Report, 86–96.

Boulogne, B., Cordier, P., and Doukhan, J.C. (1988) Defects and hydrolytic weakening in a berlinite $AlPO_4$, a structural analog of quartz. Physics and Chemistry of Minerals, 16, 250–261.

Buerger, M.J. (1956) The arrangement of atoms in crystals of the wollastonite group of metasilicates. Proceedings of the National Academy of Science, 42, 113–116.

Cameron, M., and Papike, J.J. (1980) Crystal chemistry of silicate pyroxenes. Mineralogical Society of America Reviews in Mineralogy, 7, 5–92.

Cordier, P., and Doukhan, J.C. (1989) Water in quartz, solubility and influence on ductility. European Journal of Mineralogy, 1, 221–237.

Doukhan, J.C., Doukhan, N., Nazé, L., and Van-Duysen, J.C. (1986)

Défauts de réseau et plasticité cristalline dans les pyroxènes: Une revue. Bulletin de Minéralogie, 109, 377–394.

Huebner, J.S., and Turnock, A.C. (1980) The melting relations at 1 bar of pyroxenes composed largely of Ca-, Mg-, and Fe-bearing components. American Mineralogist, 65, 225–271.

Huebner, J.S., and Voigt, D.E. (1988) Electrical conductivity of diopside: Evidence for oxygen vacancies. American Mineralogist, 73, 1235–1254.

Ingrin, J., Latrous, K., Doukhan, J.C., and Doukhan, N. (1989) Water in diopside: An electron microscopy and infrared spectroscopy study. European Journal of Mineralogy, 1, 327–341.

Ingrin, J., Doukhan, N., and Doukhan, J.C. (1991) High temperature deformation of diopside single crystals. II. TEM investigation of the defect microstructure. Journal of Geophysical Research, 96, 14287–14297.

Jaoul, O., and Raterron, P. (1993) High temperature deformation of diopside single crystals. III. Influences of P_{O_2} and SiO_2 precipitation. Journal of Geophysical Research, in press.

Jaoul, O., Houlier, B., Cheraghmakani, M., Pichon, R., and Liebermann, R.C. (1987) Surface destabilization and laboratory induced non-stoichiometry in San Carlos olivine. Physics and Chemistry of Minerals, 15, 41–53.

Kirby, S.H. (1976) The role of crystal defects in the shear-induced transformation of orthoenstatite to clinoenstatite. In H.R. Wenk, Ed., Electron microscopy in mineralogy, p. 465–472. Springer-Verlag, Berlin.

Kushiro, I. (1972) Determination of liquidus relations in synthetic silicate systems with electron probe analysis: The system forsterite-diopside-silica at 1 atmosphere. American Mineralogist, 57, 1260–1271.

——— (1973) Incongruent melting of pure diopside. Carnegie Institution of Washington Year Book, 72, 708–710.

Lange, R.A., De Yoreo, J.J., and Navrotsky, A. (1991) Scanning calorimetric measurement of heat capacity during incongruent melting of diopside. American Mineralogist, 76, 904–912.

Morse, S.A. (1980) An introduction to the quantitative use of phase diagrams in igneous petrology, 493 p. Springer-Verlag, New York.

Nakamura, A., and Schmalzried, H. (1983) On the non-stoichiometry and point defects of olivine. Physics and Chemistry of Minerals, 10, 27–37.

Nazé, L., Doukhan, N., Doukhan, J.C., and Latrous, K. (1987) A TEM study of lattice defects in naturally and experimentally deformed orthopyroxenes. Bulletin de Minéralogie, 110, 497–512.

Nitsan, V. (1974) Stability field of olivine with respect to oxidation and reduction. Journal of Geophysical Research, 79, 705–711.

Raterron, P. (1992) Fluage et fusion partielle précoce du diopside monocristallin, 193 p. Thesis, University of Paris-Sud, Orsay, France.

Raterron, P., and Jaoul, O. (1991) High temperature deformation of diopside single crystals. I. Mechanical data. Journal of Geophysical Research, 96, 14277–14286.

Richet, P., and Bottinga, Y. (1984) Anorthite, andesine, wollastonite, diopside, cordierite and pyrope: Thermodynamics of melting, glass transitions, and properties of the amorphous phases. Earth and Planetary Sciences Letters, 67, 415–432.

Richet, P., and Fiquet, G. (1991) High temperature heat capacity and premelting effects of minerals in the system MgO-CaO-Al_2O_3-SiO_2. Journal of Geophysical Research, 96, 445–456.

Richet, P., Mysen, B.O., Gillet, P., and Fiquet, G. (1992) Crystal melting: A high temperature Raman spectroscopy study. Terra Abstracts, 4, 38.

Wilkins, R.W., and Sabine, W. (1973) Water content of some nominally anhydrous silicates. American Mineralogist, 58, 508–516.

Ziegler, D., and Navrotsky, A. (1986) Direct measurement of the enthalpy of fusion of diopside. Geochimica et Cosmochimica Acta, 50, 2461–2466.

Manuscript received November 12, 1992
Manuscript accepted July 12, 1993